Three-dimensional acoustic imaging of the temporal evolution of internal wave fields in the Gulf of Mexico

Zheguang Zou[1,2], Parsa Bakhtiari Rad[2], Leonardo Macelloni[3], Likun Zhang[1,2]

[1]Department of Physics and Astronomy, University of Mississippi, University, MS 38677
[2]National Center for Physical Acoustics, University of Mississippi, 145 Hill Drive, University, MS 38677
[3]Hydrographic Science Research Center, School of Ocean Science and Engineering, The University of Southern Mississippi, 1020 Balch Blvd., Stennis Space Center, MS 39529

Key Points:

- High-resolution images of internal wave fields at the continental slope over ten days
- Resolve temporal evolution of the spatial spectra of the internal wave field
- Application of temporal variation in 3D seismic imaging for studying deep ocean dynamics

Corresponding author: Likun Zhang, `zhang@olemiss.edu`

Abstract

We report the observation of internal wave fields evolving at the continental slope in the northern Gulf of Mexico using oil-industry three-dimensional (3D) seismic imaging techniques. High-resolution seismic images reveal dynamic wave fields actively present in the 600-900 m water column. The spectral analysis of these wave fields shows that these waves possess a slope that represents the characteristics of internal waves. Further analyses suggest that these internal wave fields are most likely generated by a nearby cyclonic eddy and its interaction with the continental slope. This work demonstrates that oil-exploration 3D seismic data, if appropriately analyzed, are a useful and powerful dataset for studying the temporal evolution of deep ocean dynamics that would otherwise be impossible at similar vertical and lateral resolution.

Plain Language Summary

Waves inside the ocean, or internal waves, are difficult to visualize with traditional ocean measurements. In this study, we present high-resolution images of the internal waves in the northern Gulf of Mexico using a technique called seismic reflection imaging. In this technique, low-frequency sound signals reflected from the ocean are collected and used to reconstruct the internal structure of the ocean. We analyzed the spectrum of these structures and confirmed that they are internal waves. Moreover, we resolved the variation of the internal wave's energy spectrum over time, by taking advantage of the time information embedded in the three-dimensional seismic data. Further analysis reveals that these internal waves were most likely generated by an eddy (a large water vortex) in the Gulf of Mexico, when it approached the continental margin. This work provides a powerful tool for studying the evolution of internal waves, which would be impossible using traditional, low-resolution ocean measurements.

1 Introduction

Internal waves, or waves of the ocean interior, play an important role in the mixing and transport of freshwater, heat and nutrients in the ocean (Lamb, 2014). Internal waves are particularly active at continental margins, as they can be generated at the local continental shelf or slope, or generated remotely but reflected off or broken at the continental margins (Lamb, 2014). Generation mechanisms for internal waves include tides (Baines, 1982; Zhao et al., 2015; Zhang et al., 2017), topography (Stastna, 2011), river plumes (Nash & Moum, 2005), and other underwater disturbance (Lamb, 2014; Jackson et al., 2012). Due to different generation mechanisms, boundary conditions, and reflection angles, internal wave fields at the continental slope can be extremely complex. Prior study shows that most ocean vertical mixing does not occur in the open ocean, but at continental margins by internal waves and their interaction with the seabed topography (Polzin et al., 1997). Thus, understanding internal wave fields at continental slopes is the key for understanding vertical mixing and/or energy cascades in the global ocean.

Observing the spatial structure of internal wave fields at the continental slope is very challenging. In fact, the reconstruction of mesoscale oceanic structures in three-dimensional (3D) would require a very high vertical and horizontal sampling interval of in-situ measurements, e.g., CTD, XBT casts, mooring. For example, to reconstruct the internal wave field over a vast region, multiple one-dimensional vertical profiles would have been sampled simultaneously from different locations. Such concurrent measurements are difficult to conduct and when available, often yield poor lateral resolution (>100 m). Other in-situ measurements like underwater gliders (Rudnick et al., 2015) and floats (Furey et al., 2018) can be used for internal wave studies but they are limited to small regions. Unlike in-situ measurements, remote sensing techniques like satellite and synthetic aperture radar (SAR) can image two-dimensional (2D) surface features of internal wave solitons (Guo et al., 2012), but cannot investigate weak internal wave fields below the thermoclines which do not pro-

duce noticeable surface signature. Other remote methods include the use of high-frequency (>100 kHz) echo-sounders or ADCPs to produce high-resolution 2D acoustic image of the water column (Badiey et al., 2005), but high-frequency sound scattering is not best option for imaging internal waves because it is also subjective to enormous scatterings from microscale ocean turbulence and marine biomass (Lavery et al., 2003). Due to the difficulties of empirical observation, many studies on internal waves at the continental slope are mainly based on theory and/or modeling (Lamb, 2014). Direct observation of deep ocean dynamics are challenging and often with limited to low spatial resolutions (Rudnick et al., 2015; Furey et al., 2018).

A new and innovative approach to study mesoscale deep ocean processes is based on the use of the water-column portion of multichannel seismic data, generally collected to investigate the ocean floor subsurface. Unlike high-frequency acoustic backscattering, seismic imaging is based on acoustic reflection of low-frequency (50–200 Hz) airgun signals from the water column as a result of acoustic impedance contrast stemming from temperature and salinity distribution in the ocean (Nandi et al., 2004). Recent studies show that high-resolution images of the ocean water-column structures produced by seismic imaging can be effectively used for physical oceanographic studies (Holbrook et al., 2003; Ruddick, 2018). This establishes a new cross-discipline known as seismic oceanography (Holbrook et al., 2003). With industrial-standard marine seismic surveys, mesoscale water-column structures deeper than 200 m, e.g., ocean fronts (Liu et al., 2013; Gunn et al., 2020), eddies (Pinheiro et al., 2010), and internal waves (Holbrook & Fer, 2005; Tang et al., 2014) can be imaged with a horizontal resolution of 6.25 m and vertical resolution less than 10 m (Ruddick, 2018) depending on dominant acoustic wavelength. Seismic oceanography techniques can further resolve important ocean parameters such as turbulent and internal wave spectra (Holbrook & Fer, 2005; Krahmann et al., 2008; Holbrook et al., 2013; Sallares et al., 2016; Buffett et al., 2017; Fortin et al., 2017), diffusivity (Dickinson et al., 2017), geostrophic currents (Tang et al., 2014), and invert fundamental seawater parameters (e.g., temperature, salinity, density) with high spatial resolution (Papenberg et al., 2010). Recent study even suggested that multichannel seismic profiles acquired in 3D configuration also provide spatio-temporal information of ocean dynamics which can be useful for time-evolving oceanography studies (Zou et al., 2020). Successful applications of 3D seismic data include studying the variation of the thermocline in the north Atlantic Ocean due to an anticyclone passing by (Dickinson et al., 2020) and investigating oceanic fronts and transient lenses within the South Atlantic Ocean (Gunn et al., 2020).

This work uses 3D seismic imaging to explore the structures and spectra of time-evolving internal wave fields at the continental slope in the northern Gulf of Mexico. The 3D seismic data capture the transient nature of the internal wave fields, suggesting that local water mixing is occurring possibly as a result of the interaction of eddies with the continental slope. This wumork provides an effective tool for studying the temporal evolution of deep internal waves and the local interaction with the continental slope.

2 Data and Methods

2.1 Oceanographic Data

The study region is at the continental slope of the northern Gulf of Mexico, outside the Mississippi River delta (Fig. 1a). In this region of the Gulf, the seafloor depth varies from 600-1200 m. During the seismic surveys, CTD and XBT casts were acquired to provide concurrent in-situ oceanographic measurements to understand the vertical structure of the water column. Figure 1b shows the Temperature-Salinity (T-S) diagram based on concurrent CTD measurements collected on October 17, 2002 in our study location. Also labelled in the T-S diagram (Fig. 1b) are major types of the water masses in the region, including Caribbean Surface Water (CSW), Subtropical Underwater (SUW), Sargasso Sea Water (SSW), Tropical Atlantic Central Water (TACW), Antarctic Intermediate Water (AAIW),

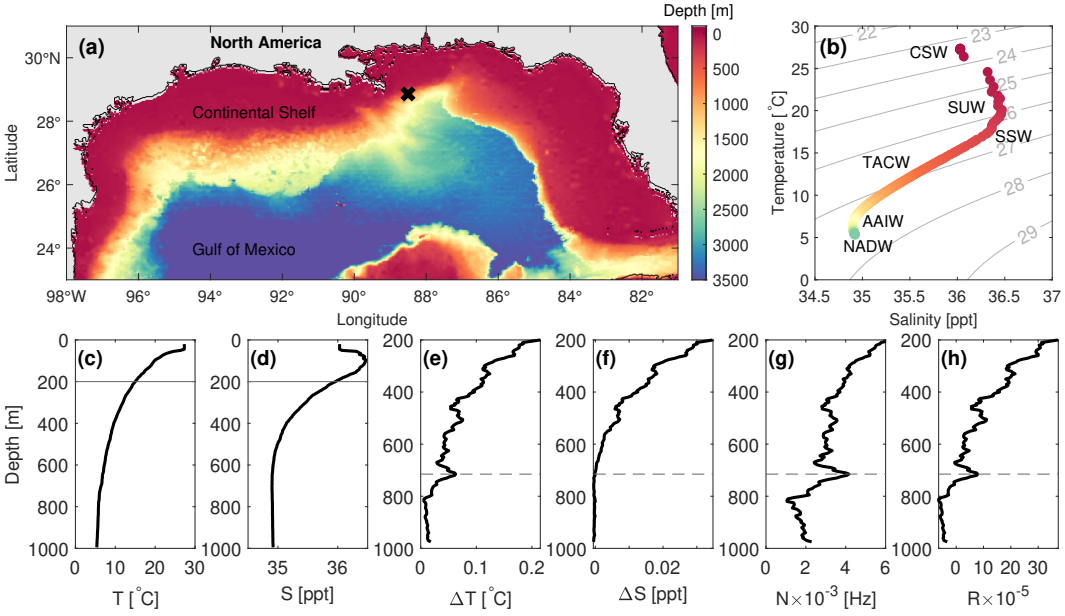

Figure 1. Topography and concurrent oceanographic data collected on October 17, 2002 at the study region in the northern Gulf of Mexico. (a) Map with seabed topography (color) and seismic survey location (cross). (b) Temperature-Salinity diagram based on concurrent (c) temperature and (d) salinity profiles. Analysis of (e) temperature gradient; (f) salinity gradient; (g) buoyancy frequency; and (h) acoustic reflection coefficient for depths of 200-1000 m. Colors in (a) and (b) represent depth, and background contour in (b) marks the potential density. Major water types listed in (b) are Caribbean Surface Water (CSW), Subtropical Underwater (SUW), Sargasso Sea Water (SSW), Tropical Atlantic Central Water (TACW), Antarctic Intermediate Water (AAIW), and North Atlantic Deep Water (NADW). The solid line in (c) and (d) and the dash line in (e)-(f) marks the depth of 200 and 715 m, respectively.

and North Atlantic Deep Water (NADW). The additional analysis with historical CTD data available in the NOAA database suggests that the T-S characteristics around this region remained unchanged over time, especially for water masses with a temperature below 20°C (corresponding to depth below 70 m). In order to make correct oceanographic interpretation for our seismic imaging, we analyzed the vertical temperature/salinity profiles, buoyancy frequency, and acoustic reflectivity for depths below 200 m (Fig. 1c-h). Results suggest that below 200 m, the acoustic reflectivity and buoyancy frequency are highly correlated with temperature difference, rather than salinity difference. In fact, the acoustic reflectivity are mostly (>99%) contributed by the vertical temperature difference in the water column (Zou et al., 2020). Therefore, the seismic intensity in our seismic images can be simply interpolated as the vertical temperature gradient. These oceanographic data were also used to build a reliable migration velocity model in our seismic data processing, and to provide the ground truth for our seismic image interpretation.

2.2 3D Seismic Data and Processing

The 3D seismic data used in this study are the water-column portion of a standard 3D high-resolution survey collected by Schlumberger WesternGeco for oil and gas exploration at the location marked in Figure 1a. The seismic vessel's sailing lines were run along the northwest-southeast direction (azimuth 330°). The seismic sources used were low-frequency, broadband airguns with a main energy band below 250 Hz in a flip-flop configuration. Eight

streamers spaced 100 m apart and accommodating 640 hydrophones at 12.5 m intervals were used to record the reflected signals. With this acquisition geometry setup, we can image the ocean structures with a resolution of 6.25 m along the sailing direction (i.e., inline direction) and 25 m perpendicular to that (i.e., crossline direction). While the vertical resolution is about 6-7 m can considering the airgun's central frequency about 60-70 Hz and the speed of sound in water about 1500 m/s.

To obtain a meaningful 3D ocean seismic volume, we have carried out a careful and data driven processing workflow because, in principle, the seismic data used are meant to target deep subsurface geological structure while water-column reflections are much weaker than both the direct wave and the seafloor reflection. Data processing was performed using both standard and non-standard techniques and details can be found in Bakhtiari Rad and Macelloni (2020). To summarize we developed a processing workflow to optimally preserve true amplitude of ocean events and to enhance water-column reflections. Data was first filtered to remove all the coherent and not coherent noise. For the imaging process, we tested both standard common-midpoint (CMP) and non-standard common reflection surface (CRS) staking. The CRS method delivered better results over the CMP method and, thus its results were considered for further analysis and interpretation. Finally, the data were time migrated and converted to depth using seismic stacking velocities estimated from semblance analysis and in situ sound velocity casts. The final result is a 3D seismic volume extending for 480 km^3 consisting of 821 inline (IL) and 3,463 crossline (XL) images.

2.3 Resolving Wave Spectrum

The spatial spectrum of the wave field can be estimated from high-resolution seismic images of the water column. The estimation is based on the assumption that seismic curvatures follow the isopycnals of the water column (Krahmann et al., 2009). Here we resolve the spatial spectrum of the internal wave fields, following the analysis techniques established in previous studies (Holbrook & Fer, 2005; Krahmann et al., 2008; Holbrook et al., 2013). The whole process include two steps.

The first step is to track all curvatures, representing internal wave fields, in the seismic image. Available tracking methods include user-guided amplitude tracking (Holbrook & Fer, 2005), cross-correlation (Krahmann et al., 2008), and instantaneous phase angle from the Hilbert transform (Holbrook et al., 2013). To improve tracking performance in small seismic images, we developed a custom tracking process based on interpolation and peak-picking. Here, seismic images are interpolated in the depth axis before tracking to yield a better spatial resolution. Then, local peaks of each seismic trace are identified with a small moving window. Finally, the local peaks in adjacent traces within a fixed depth window (e.g. 5 m) are connected. To further increase the available curvatures, we track both the positive (red) and negative (blue) peaks in the seismic images.

Once the curvatures are tracked, the second step is to estimate the spectra of the curvatures. We tested two spectral analysis methods: the Welch method (Holbrook & Fer, 2005) and the Thomson method (Dickinson et al., 2017), and results from these two methods are similar. In this work we followed most studies and used the Welch method to calculate the spatial spectra. The final spectra of the wave field is scaled by a factor of $(2\pi k_x)^2$ and plotted as a function of horizontal wave number k_x.

2.4 Resolving Temporal Variation

Resolving the temporal variation from an ocean seismic volume is one of the most important advantages for 3D seismic oceanography (Zou et al., 2020). When the ocean is sampled by typical oil-industrial 3D seismic surveys, temporal variation will appear in the crossline direction (which is perpendicular to the survey vessel's sailing direction) due to the mismatch between the timescales of ocean dynamics and the intervals of seismic surveys

(Zou et al., 2020). However, temporal variation is negligible in individual inline images, each of which only corresponds to a specific time when the seismic data were collected. Hence, a series of 3D seismic inline images can be viewed as temporally sequential snapshots, representing the evolution of the water column over time. This idea has been successfully applied to study mesoscale variability in the North Atlantic (Dickinson et al., 2020) and the ocean fronts in the South Atlantic Ocean (Gunn et al., 2020). Here we use a series of 3D inline seismic images (IL #2097-#1937) to resolve the evolution of the internal wave fields at the continental slope in the northern Gulf of Mexico during October 2002. More details about the temporal analysis of our seismic volume for this study region can be seen in Zou et al. (2020).

3 Results

A series of seismic images excerpted from our 3D seismic volume (Figure 2) show the water-column structures above the continental slope in the northern Gulf of Mexico. These images cover water column from 200 m down to the seafloor with seismic intensity represent temperature gradients or stratification levels (see Sec. 2.1). We observed that the water column was featured with highest amplitudes at 200-400 m, and lowest amplitudes at the bottom, suggesting the temperature gradient (and stratification) are strongest at 200-400 m depths, and weakest at the bottom, agreeing with the concurrent CTD data (see Figure 1e). Cross referencing these structures with concurrent CTD data and T-S diagram (Figure 1c), the corresponding water types can be identified. The highly-stratified 200-400 m water corresponds to 18°C Sargasso Sea Water (SSW), dominated by the Loop Currents. The 500-900 m water, which is less stratified with individual distinctive wave fields, corresponds to the Antarctic Intermediate Water (AAIW). The water beyond 900 m with little stratification corresponds to the North Atlantic Deep Water (NADW). The imaged seafloor ranging from 800-1000 m (with a slope of 1.9°) also matches with the topography data in this region. These preliminary analyses suggest that our seismic imaging is accurate and successfully captures the water-column structures in this region.

These sequential seismic images (Figure 2) also demonstrate the temporal evolution of the water column during October 20-27, 2002. The adjacent images here are only 0.4 km apart spatially, but 10-24 hrs apart temporally, according to the seismic data records (listed on top of each plot in Fig. 2). Notice that the 0.4-km lateral location difference is almost negligible, especially compared to the length scales of mesoscale ocean dynamics (> 10 km) (Talley et al., 2012). Hence, these images can be interpreted as the evolution of water column over time. From this perspective, the water column in this region was transitioning from a highly stratified one (with strong seismic layers) during October 20-21 (Fig. 2a-c) to less stratified one (with broken or weaker seismic layers) during October 22-27 (Fig. 2d-i). This analysis suggests that our seismic images successfully capture a drastic change in stratification of the water column, suggesting a mesoscale ocean process had occurred in this region.

More interestingly, we observed strong seismic reflections actively present at the depths of 600-900 m. Usually, at these depths, the temperature difference should be small due to low acoustic impedance contrasts in the deep ocean. However, these reflections are associated with the noticeable increase of temperature difference at the depth of 700 m (Fig. 1e), leading to increased acoustic reflectivity (Fig. 1h). We observed that, the curvatures of these seismic reflections span over a lateral distance up to 10 km with various slopes up to 1.5° (less than the 1.9° seafloor slope). Meanwhile, these wave fields are highly time-varying. The temporal scale of the wave fields must be smaller than 10 hours, which is the sampling interval in the crossline direction. Considering the study region, length scale, and time scale, such dynamic wave fields are most likely internal waves, demonstrating their interaction with the continental slope in the northern Gulf of Mexico.

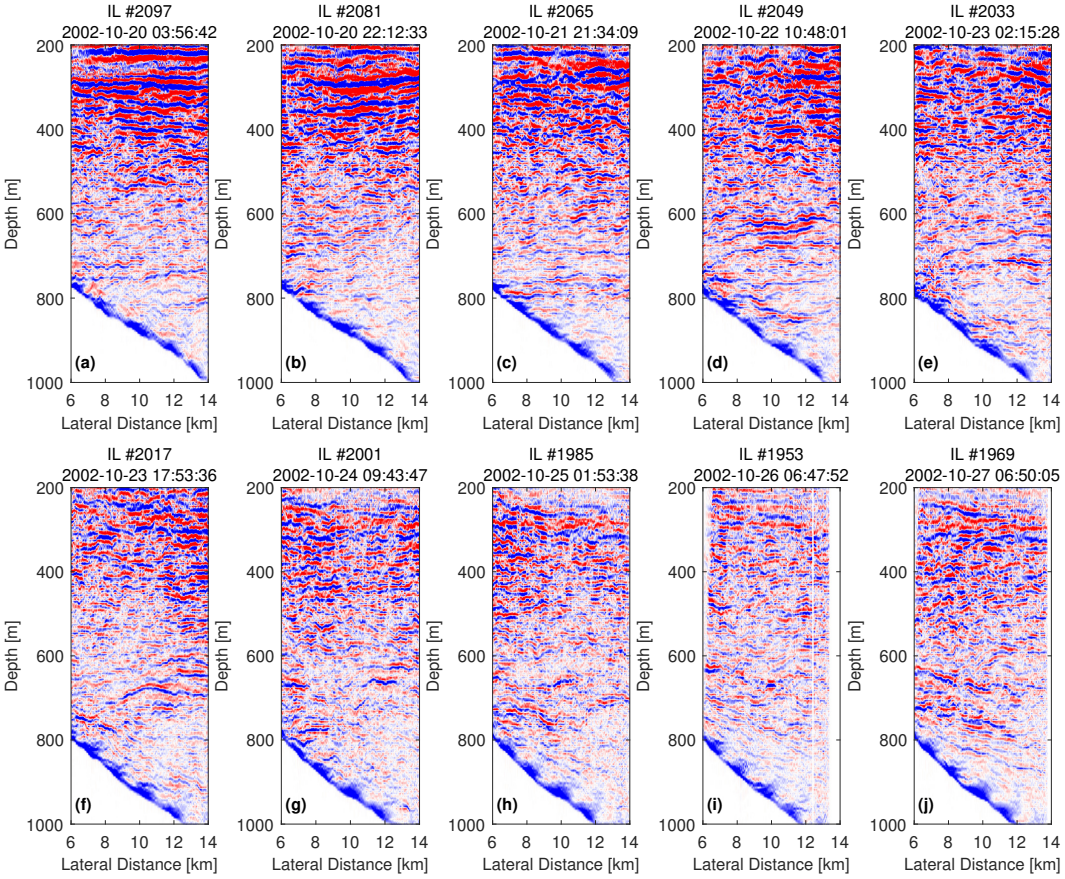

Figure 2. Seismic inline images (ILs #2097-1969) that capture the temporal evolution of the water column (200-1000 m) above the continental slope. The inline number and the data acquisition time are noted on the top. The seafloor has a slope of 1.9°.

To confirm the observation of internal waves, we analyzed the spatial spectra of the wave fields at 600-900 m, following the method described in Sec. 2.3. Figure 3a shows the original seismic images for three seismic inlines (ILs #2049, #2033, #2017). Due to the polarity of sound waves, the positive (red) and negative (blue) curvatures represent the same wave field. Therefore, to include more wave curvatures for spectral analysis, we tracked both positive and negative curvatures, and results are shown in Figure 3b. The comparison of Fig. 3a-b suggests that our tracking method successfully extracts the curvature of the wave fields, providing a clean wave curvature for spectral analysis. Finally, Figure 3c shows the averaged spatial spectra for the wave curvatures longer than 800 m at 600-900 m. Here the spectra were scaled by a factor of $(2\pi k)^2$ for a quick visual distinction between internal waves and turbulence. Theoretically, the internal waves are with a characteristic slope of -1/2, while the turbulence with slope of 1/3 (Holbrook et al., 2013; Dickinson et al., 2017). In Fig 3c, we observed that all these spectra displayed the same spectral slope, -1/2 (marked as gray curve), representing the characteristic slope of internal waves. The internal wave subrange is from 10^{-3} cpm to 10^{-1} cpm. Three inlines show slightly different wave energy levels. This spectral analysis confirms the observation of internal waves fields in our seismic images, and the spectral variation suggests a change in internal wave energy between these three inlines.

Finally, we demonstrated the evolution of the internal wave fields during October 20-29 by applying the spectral analysis to the whole inline series (ILs #2097-1969, Fig. 4). The

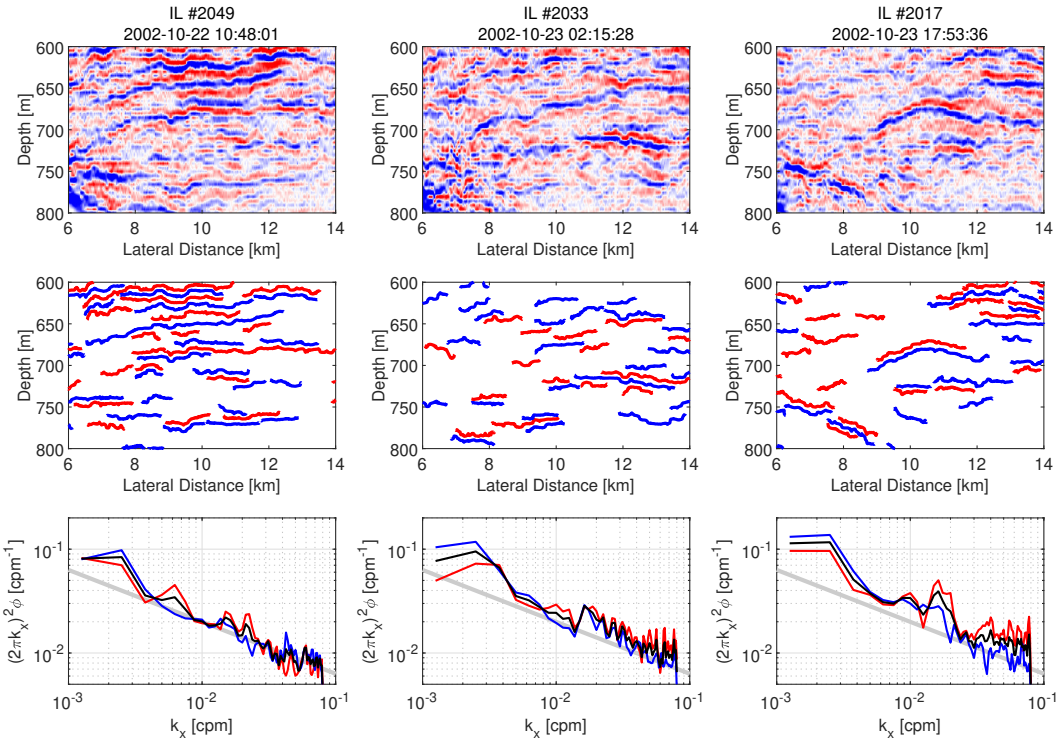

Figure 3. Spectral analysis of wave curvatures (at 600-800 m) in seismic images (ILs #2049, #2033, #2017). (Top) Original seismic images (with inline and time marked on top). (Middle) Extracted positive (red) and negative (blue) seismic curvatures. (Bottom) The positive (red), negative (blue) and average (black) slope spectra estimated from tracked curvatures. The characteristic internal wave slope (-1/2) is marked by the grey curve.

observation of internal waves during the whole period is confirmed from the *slope* view of the wave spectra (Fig. 4a), which displays the same -1/2 internal wave slope (black curve). Meanwhile, a *temporal* view of the same wave spectra is shown in Fig. 4b, in which the wave spectra were interpolated and plotted as a function of time. This temporal view of the spatial wave spectra illustrates the temporal evolution of the internal wave fields' spectral energy during October 20-29, 2002. We observed that the internal wave energy decreased to a minimum on October 22, gradually increased and reached a maximum on October 26. This increased internal wave energy may imply an intensified water mixing and a decrease of water-column stratification. Our spectral analysis of the whole inline series provides a spatio-temporal picture of the evolution of the internal wave fields' energy for understanding the local ocean dynamics.

4 Discussion

Our results shed a light on the mesoscale ocean dynamics and the generation mechanism of the internal wave fields in this region. One one hand, our seismic images show a drastic change in the vertical structure of the water column with reduced stratification (Fig. 2), implying a mesoscale oceanographic process occurred in this region that had increased the vertical mixing. On the other hand, our temporal view of the wave spectra shows intensified internal wave energy during the same period (Fig. 4), also suggesting increased vertical mixing. Given this coincidence, it is possible that the mesoscale ocean process occurring in this region generated these internal waves, which increased the water mixing and eventually

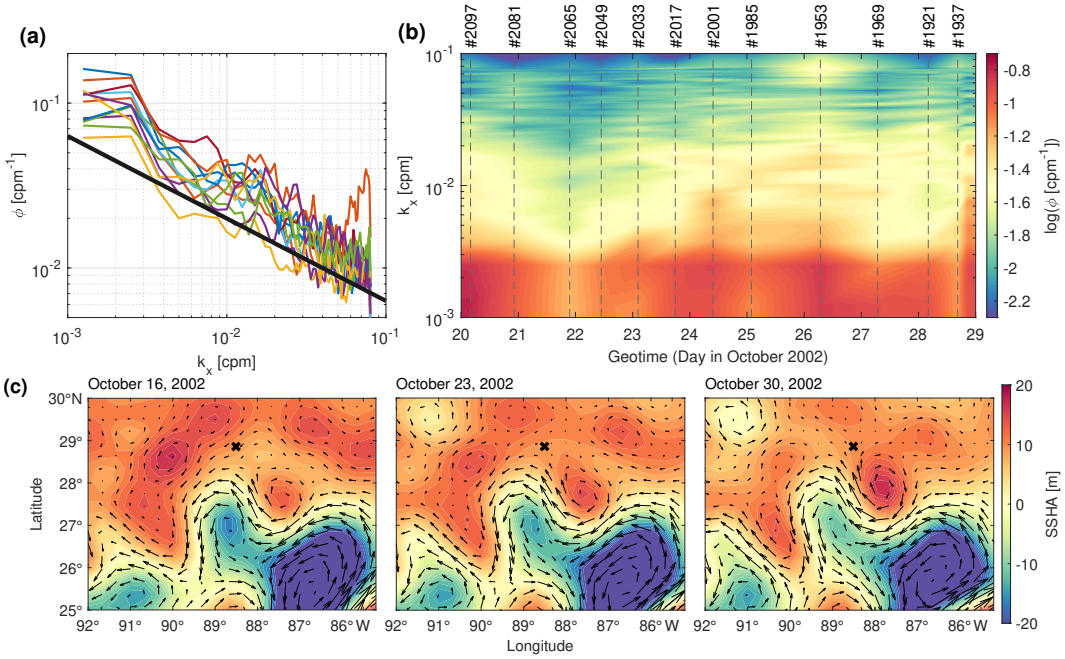

Figure 4. The evolution of the spectrum of deep internal waves during October 20-29, 2002. (a) Slope view. (b) Temporal view (interpolated). The solid black curve marks the internal wave characteristic slope. The color code represents the slope spectral amplitude in logarithmic scale. The spectra are for the waves deeper than 500 m. The inline number is denoted on the top. (c) Weekly satellite images of sea surface height anomaly (color) with surface geostrophic currents (arrow) during October 16-30, 2002.

changed the water-column stratification. Here we discuss possible ocean dynamics and generation mechanisms for the internal wave fields observed in our seismic imaging.

The water dynamics in this region of the Gulf is mainly dominated by the Loop Currents and the Mississippi River outflows (Coleman, 1988; Sturges & Lugo-Fernandez, 2005). Possible mesoscale oceanographic processes that may occur in this region include river plumes due to the Mississippi River discharge (Lohrenz et al., 1997), oceanic fronts along the Louisiana-Texas continental shelf (Belkin et al., 2009), eddies and meanders due to Loop Currents (Rudnick et al., 2015), and internal waves and flows above the continental slope (Rubenstein, 1999; Dickinson et al., 2017). Possible mechanisms that can generate internal waves in this region include tides (Lamb, 2014), river plumes (Nash & Moum, 2005), and eddies (Clément et al., 2016). Preliminary examination of the dimensional scales of these processes suggests that all these dynamics can be observed (fully or partially) by seismic reflection imaging techniques.

Among these possible dynamics, the internal wave fields seen in our seismic imaging were most likely generated by eddies, rather than tides or river plumes. Tidal dynamics are mainly associated with semidiurnal or diurnal cycles (12 or 24 hrs), but our spectral analysis (Fig. 4b) suggests that the generation source demonstrated a temporal pattern longer than eight days (October 20-27, 2002), way beyond main tidal cycles. Mississippi River plumes are often restricted to the continental shelf due to the seasonal-shifting eastwards or westwards along-shelf surface currents, and have little impact on the depths below the thermoclines (Walker, 1996; Schiller et al., 2011). For these reasons, internal waves in this case are most likely generated by eddies. Cyclonic and anticyclonic eddies, prevalent in the Gulf and associated with a variety of timescale from several days to months, can generate internal

waves when interacting with the continental slope (Hamilton & Lee, 2005). To further confirm the presence of eddies during the seismic survey, we analyzed the historical satellite data. Figure 4c shows the weekly satellite images for sea surface height anomaly along with estimated surface geostrophic currents, suggesting that there was a strong cyclonic frontal eddy (Loop Current Frontal Eddy, LCFE) approaching our seismic region during the week of October 25, 2002.

Based on these analyses, the possible dynamics and mechanisms are explained as follows. The Loop Currents create omnipresent cyclonic and anticyclonic eddies moving northward and eastward in the Gulf. When eddies approach the northern continental margin, they start to interact with the seafloor topography, generating internal waves at the continental slope. This process converted the mesoscale eddy energy to submesoscale internal wave energy, increased the vertical water mixing, and reduced the stratification of the water column. Particularly in our study region, the generated internal waves were likely to be focused by the V-shaped Mississippi Canyon, causing internal waves to reflect off or break near the continental slope (Hotchkiss & Wunsch, 1982; Ross et al., 2009). Hence, our seismic images (Fig. 2) and spatio-temporal spectra (Fig. 4) in this work demonstrate the complex process of the interaction between eddies, internal waves, and the continental slope, as well as the mechanisms of wave generation, reflection and breaking.

5 Conclusions

In this letter, we presented seismic images and spectra to illustrate temporal evolution of internal wave fields at the continental slope in the Gulf of Mexico over ten days. Our analysis suggested that these internal waves were most likely generated by the interaction of eddies with the continental slope, including various mechanisms like generation, reflection and breaking of internal waves. This work showcases the power of 3D seismic oceanography, and provides an effective tool to study the temporal evolution of deep ocean dynamics. The internal wave fields' spatio-temporal spectra resolved in this work cannot be resolved from 2D seismic imaging due to the lack of temporal variation, or from traditional oceanographic measurements due to their low lateral spatial resolutions. Our future 3D seismic oceanography research will focus on using the 3D seismic reflection imaging to understand complex water dynamics in the Gulf of Mexico.

Acknowledgments

We would like to thank Schlumberger WesternGeco for providing 3D seismic data. These data are available from Schlumberger Multiclient Seismic Data Library (http://www.multiclient.slb.com; area MC-14Q). The seismic data were processed with software Vista from Schlumberger, Kingdom by IHS Markit, Seismic Unix from Colorado School of Mines. The satellite data are from Asia-Pacific Data-Research Center (http://apdrc.soest.hawaii.edu/data/). This work was supported by the National Oceanic and Atmospheric Administration (NOAA) grant # NA17OAR011021.

References

Badiey, M., Katsnelson, B. G., Lynch, J. F., Pereselkov, S., & Siegmann, W. L. (2005). Measurement and modeling of three-dimensional sound intensity variations due to shallow-water internal waves. *The Journal of the Acoustical Society of America*, *117*(2), 613–625. doi: 10.1121/1.1828571

Baines, P. G. (1982). On internal tide generation models. *Deep Sea Research Part A. Oceanographic Research Papers*, *29*(3), 307–338.

Bakhtiari Rad, P., & Macelloni, L. (2020). Improving 3D water column seismic imaging using the Common Reflection Surface method. *Journal of Applied Geophysics*, *179*, 104072. Retrieved from `https://doi.org/10.1016/j.jappgeo.2020.104072` doi:

10.1016/j.jappgeo.2020.104072

Belkin, I. M., Cornillon, P. C., & Sherman, K. (2009). Fronts in large marine ecosystems. *Progress in Oceanography*, *81*(1-4), 223–236.

Buffett, G. G., Krahmann, G., Klaeschen, D., Schroeder, K., Sallarès, V., Papenberg, C., ... Zitellini, N. (2017). Seismic oceanography in the Tyrrhenian Sea: thermohaline staircases, eddies, and internal waves. *Journal of Geophysical Research: Oceans*, *122*(11), 8503–8523. doi: 10.1002/2017JC012726

Clément, L., Frajka-Williams, E., Sheen, K., Brearley, J., & Garabato, A. N. (2016). Generation of internal waves by eddies impinging on the western boundary of the north atlantic. *Journal of Physical Oceanography*, *46*(4), 1067–1079.

Coleman, J. M. (1988). Dynamic changes and processes in the mississippi river delta. *Geological Society of America Bulletin*, *100*(7), 999–1015.

Dickinson, A., White, N. J., & Caulfield, C. P. (2017). Spatial variation of diapycnal diffusivity estimated from seismic imaging of internal wave field, Gulf of Mexico. *Journal of Geophysical Research: Oceans*, *122*(12), 9827–9854. doi: 10.1002/2017JC013352

Dickinson, A., White, N. J., & Caulfield, C. P. (2020). Time-Lapse Acoustic Imaging of Mesoscale and Fine-Scale Variability within the Faroe-Shetland Channel. *Journal of Geophysical Research: Oceans*. doi: 10.1029/2019jc015861

Fortin, W. F., Holbrook, W. S., & Schmitt, R. W. (2017). Seismic estimates of turbulent diffusivity and evidence of nonlinear internal wave forcing by geometric resonance in the South China Sea. *Journal of Geophysical Research: Oceans*, *122*(10), 8063–8078. doi: 10.1002/2017JC012690

Furey, H., Bower, A., Perez-Brunius, P., Hamilton, P., & Leben, R. (2018). Deep eddies in the gulf of mexico observed with floats. *Journal of Physical Oceanography*, *48*(11), 2703–2719.

Gunn, K. L., White, N., & Caulfield, C. c. P. (2020). Time-Lapse Seismic Imaging of Oceanic Fronts and Transient Lenses Within South Atlantic Ocean. *Journal of Geophysical Research: Oceans*, *125*(7), 1–26. doi: 10.1029/2020JC016293

Guo, C., Vlasenko, V., Alpers, W., Stashchuk, N., & Chen, X. (2012). Evidence of short internal waves trailing strong internal solitary waves in the northern south china sea from synthetic aperture radar observations. *Remote sensing of environment*, *124*, 542–550.

Hamilton, P., & Lee, T. N. (2005). Eddies and jets over the slope of the northeast Gulf of Mexico. In *Circulation in the gulf of mexico* (pp. 123–142). Washington DC: The American Geological Union.

Holbrook, W. S., & Fer, I. (2005). Ocean internal wave spectra inferred from seismic reflection transects. *Geophysical Research Letters*, *32*(15), 2–5. doi: 10.1029/2005GL023733

Holbrook, W. S., Fer, I., Schmitt, R. W., Lizarralde, D., Klymak, J. M., Helfrich, L. C., & Kubichek, R. (2013). Estimating oceanic turbulence dissipation from seismic images. *Journal of Atmospheric and Oceanic Technology*, *30*(8), 1767–1788. doi: 10.1175/JTECH-D-12-00140.1

Holbrook, W. S., Páramo, P., Pearse, S., & Schmitt, R. W. (2003). Thermohaline fine structure in an oceanographic front from seismic reflection profiling. *Science*, *301*(5634), 821–824. doi: 10.1126/science.1085116

Hotchkiss, F. S., & Wunsch, C. (1982). Internal waves in hudson canyon with possible geological implications. *Deep Sea Research Part A. Oceanographic Research Papers*, *29*(4), 415–442.

Jackson, C. R., Da Silva, J. C., & Jeans, G. (2012). The generation of nonlinear internal waves. *Oceanography*, *25*(2), 108–123.

Krahmann, G., Brandt, P., Klaeschen, D., & Reston, T. (2008). Mid-depth internal wave energy off the Iberian Peninsula estimated from seismic reflection data. *Journal of Geophysical Research: Oceans*, *113*(C12), C12016. Retrieved from `http://doi.wiley.com/10.1029/2007JC004678` doi: 10.1029/2007JC004678

Krahmann, G., Papenberg, C., Brandt, P., & Vogt, M. (2009). Evaluation of seis-

mic reflector slopes with a Yoyo-CTD. *Geophysical Research Letters*, *36*(August), L00D02. Retrieved from http://doi.wiley.com/10.1029/2009GL038964 doi: 10.1029/2009GL038964

Lamb, K. G. (2014). Internal Wave Breaking and Dissipation Mechanisms on the Continental Slope/Shelf. *Annual Review of Fluid Mechanics*, *46*(1), 231–254. Retrieved from http://www.annualreviews.org/doi/10.1146/annurev-fluid-011212-140701 doi: 10.1146/annurev-fluid-011212-140701

Lavery, A. C., Schmitt, R. W., & Stanton, T. K. (2003). High-frequency acoustic scattering from turbulent oceanic microstructure: The importance of density fluctuations. *The Journal of the Acoustical Society of America*, *114*(5), 2685. Retrieved from http://scitation.aip.org/content/asa/journal/jasa/114/5/10.1121/1.1614258 doi: 10.1121/1.1614258

Liu, H., Hu, Y., Yin, Y., Wang, L., Tong, S., & Ma, H. (2013). Shallow Water Body Data Processing Based on the Seismic Oceanography. *Journal of Ocean University of China*, *12*(3), 319–326. doi: 10.1007/s11802-013-2100-5

Lohrenz, S. E., Fahnenstiel, G. L., Redalje, D. G., Lang, G. A., Chen, X., & Dagg, M. J. (1997). Variations in primary production of northern gulf of mexico continental shelf waters linked to nutrient inputs from the mississippi river. *Marine Ecology Progress Series*, *155*, 45–54.

Nandi, P., Holbrook, W. S., Pearse, S., Páramo, P., & Schmitt, R. W. (2004). Seismic reflection imaging of water mass boundaries in the Norwegian Sea. *Geophysical Research Letters*, *31*(23), 1–4. doi: 10.1029/2004GL021325

Nash, J. D., & Moum, J. N. (2005). River plumes as a source of large-amplitude internal waves in the coastal ocean. *Nature*, *437*(7057), 400–403. doi: 10.1038/nature03936

Papenberg, C., Klaeschen, D., Krahmann, G., & Hobbs, R. W. (2010). Ocean temperature and salinity inverted from combined hydrographic and seismic data. *Geophysical Research Letters*, *37*(4). doi: 10.1029/2009GL042115

Pinheiro, L. M., Song, H., Ruddick, B., Dubert, J., Ambar, I., Mustafa, K., & Bezerra, R. (2010). Detailed 2-D imaging of the Mediterranean outflow and meddies off W Iberia from multichannel seismic data. *Journal of Marine Systems*, *79*(1-2), 89–100. Retrieved from http://dx.doi.org/10.1016/j.jmarsys.2009.07.004 doi: 10.1016/j.jmarsys.2009.07.004

Polzin, K., Toole, J., Ledwell, J., & Schmitt, R. (1997). Spatial variability of turbulent mixing in the abyssal ocean. *Science*, *276*(5309), 93–96.

Ross, C. B., Gardner, W. D., Richardson, M. J., & Asper, V. L. (2009). Currents and sediment transport in the Mississippi Canyon and effects of Hurricane Georges. *Continental Shelf Research*, *29*(11-12), 1384–1396. doi: 10.1016/j.csr.2009.03.002

Rubenstein, D. (1999). Observations of cnoidal internal waves and their effect on acoustic propagation in shallow water. *IEEE journal of oceanic engineering*, *24*(3), 346–357.

Ruddick, B. R. (2018). Seismic oceanography's failure to flourish: a possible solution. *Journal of Geophysical Research: Oceans*, *123*(1), 4–7. doi: 10.1002/2017JC013736

Rudnick, D. L., Gopalakrishnan, G., & Cornuelle, B. D. (2015). Cyclonic eddies in the gulf of mexico: Observations by underwater gliders and simulations by numerical model. *Journal of Physical Oceanography*, *45*(1), 313–326.

Sallares, V., Mojica, J. F., Biescas, B., Klaeschen, D., & Gràcia, E. (2016). Characterization of the submesoscale energy cascade in the Alboran Sea thermocline from spectral analysis of high-resolution MCS data. *Geophysical Research Letters*, *43*(12), 6461–6468. doi: 10.1002/2016GL069782

Schiller, R. V., Kourafalou, V. H., Hogan, P., & Walker, N. D. (2011, June). The dynamics of the Mississippi River plume: Impact of topography, wind and offshore forcing on the fate of plume waters. *Journal of Geophysical Research*, *116*(C6), C06029. Retrieved 2020-10-20, from http://doi.wiley.com/10.1029/2010JC006883 doi: 10.1029/2010JC006883

Stastna, M. (2011). Resonant generation of internal waves by short length scale topography. *Physics of Fluids*, *23*(11), 116601.

Sturges, W., & Lugo-Fernandez, A. (Eds.). (2005). *Circulation in the Gulf of Mexico: Observations and Models*. Washington, D. C.: American Geophysical Union. Retrieved 2020-10-04, from http://doi.wiley.com/10.1029/GM161 doi: 10.1029/GM161

Talley, L. D., Pickard, G. L., Emery, W. J., & Swift, J. H. (2012). Introduction to Descriptive Physical Oceanography. *Descriptive Physical Oceanography*, 1–6. doi: 10.1016/b978-0-7506-4552-2.10001-0

Tang, Q. S., Gulick, S. P. S., & Sun, L. T. (2014). Seismic observations from a Yakutat eddy in the northern Gulf of Alaska. *Journal of Geophysical Research: Oceans*, *119*, 3535–3547. doi: 10.1002/2014JC009938

Walker, N. D. (1996, October). Satellite assessment of Mississippi River plume variability: Causes and predictability. *Remote Sensing of Environment*, *58*(1), 21–35. Retrieved 2020-10-20, from https://linkinghub.elsevier.com/retrieve/pii/0034425795002596 doi: 10.1016/0034-4257(95)00259-6

Zhang, L., Buijsman, M. C., Comino, E., & Swinney, H. L. (2017). Internal wave generation by tidal flow over periodically and randomly distributed seamounts. *Journal of Geophysical Research: Oceans*, *122*(6), 5063–5074.

Zhao, J., Zhang, L., & Swinney, H. L. (2015). Topographic height dependence of internal wave generation by tidal flow over random topography. *Geophysical Research Letters*, *42*(19), 8081–8087.

Zou, Z., Bakhtiari Rad, P., Macelloni, L., & Zhang, L. (2020). Temporal and Spatial Variations in Three-Dimensional Seismic Oceanography. *Ocean Science*(under review).